

# Multigrid method for quantum transport in molecular electronic devices

Guogang Feng<sup>1</sup>, Thomas L. Beck<sup>1\*</sup>, Nimal Wijesekera<sup>2</sup>

<sup>1</sup>*Department of Chemistry*

<sup>2</sup>*Department of Physics  
University of Cincinnati*

*Cincinnati, OH 45221-0172*

thomas.beck@uc.edu

\*corresponding author

February 28, 2005

## Abstract

We report a self-consistent *ab initio* method to calculate quantum transport through a molecule connected to gold electrodes under an applied current. This method is based on the density-functional theory(DFT) with a current constrained term as an imaginary potential in the Hamiltonian. Pseudopotentials are used to define atomic cores. The open and nonequilibrium system is reduced to a closed system. We treat both the molecule and the electrodes on the same footing as an extended molecule. Multigrid technique is used to accelerate convergence in a local optimized-orbital basis. Landauer formula is used to calculate the bias with transmission coefficient obtained from the Green's function. The current-voltage characteristics of a benzene-1,4-dithiolate(BDT) extended molecule is studied and our results are comparable to other theoretical calculations. This efficient method provides another way to study the quantum transport of molecule electronic devices.

## Introduction

As the miniaturization of conventional silicon-based microelectronic devices proceeds, the molecule scale will be reached within a decade. Molecular electronics is a promising field because of their small size, light weight, low cost, synthetic adaptability and nontoxicity. There are considerable achievements in the experiments. For example, the current-voltage( $I - V$ ) characteristics of a benzene-1,4-dithiolate(BDT) molecule sandwiched between two gold(111) electrodes has been measured [1], molecular diodes [2, 3], switches [3] and memory elements [4] have been fabricated.

On the theoretical side, the effective-mass approximation which works for traditional electron transport in the bulk semiconductor devices breaks down in the molecular level. Quantum effects play a dominant role in the molecular electronic devices. Landauer-Büttiker formalism [5, 6, 7] has been extensively used in quantum transport through molecular systems. The Landauer approach assumes the transport to be coherent, the scattering in the

molecule is elastic, there are no incoherent and inelastic processes.

Extensive effort [8, 9, 10, 11, 12, 13, 14, 15, 16, 17, 18] has been directed at understanding the fundamental physics and chemistry of transport through molecules attached on either side to a metal contact. These theoretical works have led to a great insight into the origins of the transport in molecular devices. However, these studies involve approximations which include the extended-Huckel-level of theory, cluster models, incomplete treatment of the influence of the metal contacts, lack of accurate description of the electronic structure.

Recently, Lang and coworkers [19, 20, 21] have developed a method for self-consistent determination of current-voltage characteristics of molecular wires using density functional theory(DFT) [22] in plane-wave basis set. In this method, the electrodes are treated as ideal metals where the electron states are populated up to the Fermi level. Incoming and outgoing plane-wave states are included in addition to the molecular states. The Lippmann-Schwinger equation is used to solve the wave functions self-consistently in the scattering formalism under a given bias. The main advantages of this approach are as follows. 1) The open system is handled by proper boundary conditions. 2) The influence of the applied bias on the molecule levels is included. 3) The effective potential is obtained self-consistently. The drawback is that the simple jellium model for electrodes neglects the surface effects such as chemisorption and bonding with the contacts.

Another way to study the electron transport in molecular electronic devices is combining the nonequilibrium Green function(NEGF) [23, 24, 25, 26, 27, 28, 29] with DFT. In this method, open boundary conditions and the influence of the applied bias to drive the system to nonequilibrium conditions can be treated rigorously. The nonequilibrium Green function matrix naturally include both scattering states and bound states contribution to the charge density. The jellium model is dropped. The metallic screening in the electrodes limits the charge and potential induced by the adsorption of the molecule to extend over only a finite region into the electrodes [25]. So the molecule and the electrodes in that finite region are treated explicitly on the same footing as an extended molecule. Either 3 [24] or 6 [26] gold atoms in each electrode are included as an extended molecule for electrode-BDT-electrode system. Current-voltage curves are calculated for the electrode-BDT-electrode system fully self-consistently [26, 29]. The nonequilibrium Green function matrix demands extensive computer resources in a large bias even performing energy integration in the complex contour. Therefore the numerical method for NEGF coupled to DFT implementation has to be chosen carefully. The main difference in the previous implementations are the choice of basis functions, such as atomic orbitals [23, 29] and Gaussian orbitals [24, 26, 27].

The fully self-consistent NEGF coupled to DFT is computationally expensive, some groups have developed approximate methods [30, 31] to calculate the current-voltage curves for the BDT extended molecule. Derosa and Seminario [30] have performed the quantum DFT calculation under an external field by using commercial Gaussian-98 program [32] where the charge effect from scattering states are neglected. Tomfohr and Sankey [31] have performed the DFT calculation at zero voltage, they do not include the charge effect from scattering states and bias induced in the electronic structure. They make a voltage shift when performing the current calculation. The above two calculations are fast but approximate, so

a high efficient and accurate method is highly desirable.

Conventional DFT can be applied to closed or periodic systems in quantum chemistry and physics. It needs to be modified in order to apply to the electronic transport through an open and nonequilibrium quantum system. Along this line, we modify our multigrid DFT solver [33, 34] by adding a current constrained term [35, 36, 37] in Kohn-Sham Hamiltonian.

The discretization in DFT for large-scale electronic structure calculations can be in atomic basis [38, 39], plane-wave basis [40], and real-space [41]. Our multigrid DFT solver is in real space finite difference representation. Due to the localized nature of the DFT Hamiltonian operator in real space, it has several advantages. First, the efficient multigrid technique can be applied to accelerate convergence. Second, natural localization constraint on the orbital can be imposed in searching linear scaling algorithms [42, 43]. Third, when it is running in the parallel codes, a less traffic of data distributes among processors. Finally, local mesh refinements can be incorporated efficiently [44, 45]. Many real space multigrid DFT solvers have been developed [43, 44, 46, 47, 48, 49, 50, 51, 52].

The electronic transport calculations under the applied bias in open quantum system can be conceptually circumvented by current given instead of the applied bias. The current constrained term [35, 36, 37] is an imaginary anticommutator obtained from Lagrange multiplier approach. This additional imaginary potential forces the wave functions complex to insure the current constraint but still keeps the Hamiltonian Hermitian, thus real eigenvalues in a closed system. The current is assumed to be a steady current through the molecular electronic device in one direction, the region of the current is restricted by a step function according to the molecular device boundaries. In this modified DFT, the electronic correlations are considered at the same level as they are in the conventional DFT [37]. By using this modified DFT, the charge effect due to the scattering states and the applied bias is properly handled in a closed system. The electronic potential profile and complex wave functions can be obtained fully self-consistently. From Landauer formula, the potential bias can be determined if the transmission coefficient is known.

There are several methods to calculate the transmission coefficient in quantum devices such as the transfer matrix method[53, 54, 55, 56], the quantum transmitting boundary methods [57, 58], the contact block reduction method [59], the wave-function matching method[60, 61, 62], and the Green's function method[23, 24, 25, 26, 27, 28, 29, 30, 31, 63, 64].

The transfer matrix method is unstable for a large system, numerical errors may blow up exponentially in the matrix elements of the recursive multiplication transfer matrices. This numerical instability is due to the exponentially growing and decaying evanescent waves[54, 55]. When the pseudopotential approach is used, the transfer matrix method is complicated and computationally expensive to handle the nonlocal pseudopotential[55].

The quantum transmitting boundary method developed by Frensley[57] and Lent et al. [58] is to solve linear equations self-consistently that match the open boundary conditions which can not determined until the full solution is found. It is computationally expensive. It has not been applied to three-dimensional calculation yet.

The contact block reduction method developed by Mamaluy et al.[59] is to express the transmission function in terms of a small submatrix of the retarded Green's function of the

open device. The transmission function can be approximately calculated with an incomplete set of eigenstates of the closed system. The relation between accuracy and the number of eigenvalues depends on the structure.

The wave-function matching method is as follows. The whole system is divided by three parts, left and right semi-infinite bulk leads and a scattering region. All propagating and evanescent Bloch wave functions in the leads are calculated first, then the scattering wave functions match the Bloch wave-function of the leads near boundary values. This process leads to the Green's function matrix which contains the transmission coefficient. This method is limited to the local pseudopotential only [60, 61], the inclusion of the nonlocal part of the pseudopotential will need further work.

The transmission coefficient can be calculated by the Green's function method. For the molecule sandwiched between two semi-infinite metallic electrodes, the Green's function describes the dynamics of the electrons inside the molecule, taking the effect of the electrodes into account through the coupling of the molecule to the electrodes [63]. Although the Green's function for the whole system has infinite dimensions in matrix form, it can be expressed in a finite matrix under localized basis [23, 24, 25, 26, 27, 28, 29, 30, 31, 63, 64]. We will use the Green's function in local optimized-orbital basis [43, 64] to get the transmission coefficient.

The remainder of this paper is organized as follows. A detailed description of the theoretical formalism is given in section II. DFT with current constrained term is described first, how we implement the multigrid DFT in the optimized-orbital is discussed next, finally, the Green's function in the optimized-orbital basis is given. Section III presents numerical results for the BDT extended molecule and Section IV summarizes the paper.

## Theoretical Formalism

### *DFT with a current constrained term*

The Kohn-Sham equations with a current constrained term is given as follows [37]:

$$-\frac{1}{2}\nabla^2\psi_j(\mathbf{r}) + v_{eff}\psi_j(\mathbf{r}) + \int v_{nl}(\mathbf{r}, \mathbf{r}')\psi_j(\mathbf{r}')d\mathbf{r}' - \frac{1}{2i}\left[\frac{I(x)}{\rho_{yz}(x)}, \frac{\partial}{\partial x}\right]_+\psi_j(\mathbf{r}) = \lambda_j\psi(\mathbf{r}), \quad (1)$$

where

$$v_{eff} = v_H + v_{xc} + v_{local}. \quad (2)$$

The Hartree potential  $v_H$  satisfies the Poission equation,

$$\nabla^2v_H = -4\pi\rho(x, y, z). \quad (3)$$

The exchange-correlation potential  $v_{xc}$  is in local density approximation(LDA) VWN form [65].  $v_{local}$  and  $v_{nl}$  are the local and nonlocal pseudopotential developed by Goedecker *et al.* [66, 67], respectively. They have analytic forms in the separable dual-space. We use the real-space relativistic version of these pseudopotentials for our calculations.

$I(x)$  and  $\rho_{yz}(x)$  in Eq.(1) are given as follows:

$$I(x) = I \theta(x - L, R - x) , \quad (4)$$

$$\rho_{yz}(x) = \int dy dz \rho(x, y, z) . \quad (5)$$

$I$  is the steady current through the system in  $yz$  plane,  $L$  and  $R$  are the left and right boundaries of the system in  $x$  direction, respectively.  $\theta$  is the step function.

Eq.(1) is Hermitian [37], eigenvalue  $\lambda$  is real but wavefunction  $\psi$  is complex. The anti-commutator term in Eq.(1) is the additional imaginary potential arising from the constraint current. With introduction of this term, the scattering states of an open quantum system can be described in terms of wave functions of an effectively closed system. We will solve Kohn-Sham equations by the multigrid method in local optimized-orbital basis.

### *Optimized-orbital basis*

The Kohn-Sham equations can be solved in real space by traditional Ritz procedure [33], where the Gram-Schmidt orthogonalization scales as  $O(N^3)$ , where  $N$  is the number of wave functions. It can be improved by employing the optimized nonorthogonal orbitals developed by Fattebert *et al.* [43]. Their ideas are as follows. The wave functions are described in the basis of eigenfunctions with a localization constraint. The constraint requires that a wave function is set zero outside a prescribed spherical region. The local optimized-orbital basis is nonorthogonal in general. The radius of the sphere is chosen by numerical tests, and the center of the sphere is atom-centered. In their implementation, they use a multigrid preconditioner to improve the steepest descent directions in the relaxation. They also impose orthogonal condition for the wave functions localized on the same atom. We follow their ideas but implement differently. Our implementation is more efficient as follows. We solve the Kohn-Sham equations in the optimized-orbital basis by the multigrid method, and we do not impose the orthogonal condition for the wave functions localized on the same atom.

Let  $N$  denote the number of wave functions and  $M$  the number of grid points discretized for the Kohn-Sham equations. An orthogonal basis of wave functions in Ritz procedure can be written in a column matrix  $\Psi = (\psi_1, \dots, \psi_N)$ . We want to solve  $\Psi$  in a normalized nonorthogonal basis  $\Phi = (\phi_1, \dots, \phi_N)$ . We use a  $N \times N$  matrix  $C$  to transform  $\Phi$  into  $\Psi$ ,

$$\Psi = \Phi C . \quad (6)$$

$C$  is a solution of the generalized complex eigenvalue problem

$$H^{(\Phi)} C = S C \Lambda , \quad (7)$$

where  $H^{(\Phi)} = \Phi^\dagger H \Phi$  is the Hamiltonian integration in the  $\Phi$  basis,  $S = \Phi^\dagger \Phi$  is the overlap matrix, and  $\Lambda$  is the diagonal eigenvalue.

The electronic density  $\rho(\mathbf{r})$  is given by

$$\rho(\mathbf{r}) = 2 \sum_{j,k=1}^N \sqrt{|(S_{jk}^{-1}) \phi_j(\mathbf{r})^\dagger \phi_k(\mathbf{r})|^2}. \quad (8)$$

The nonorthogonal orbital  $\Phi$  converges along the steepest descent direction as follows:

$$D^{(\Phi)} = \Phi \Theta - H \Phi, \quad (9)$$

where  $\Theta = S^{-1} H^{(\Phi)}$ .

In a multigrid  $k$  level, Eq.(9) has the following form,

$$H^k \Phi^k = \Phi^k \Theta^k + \tau^k, \quad (10)$$

where  $\tau^k$  is the defect correction in  $k$  level defined as

$$\begin{aligned} \tau^k = I_{k+1}^k \tau^{k+1} + H^k \left( I_{k+1}^k \Phi^{k+1} \right) - \left( I_{k+1}^k \Phi^{k+1} \right) \Theta^k \left( I_{k+1}^k \Phi^{k+1} \right) \\ - I_{k+1}^k \left[ H^{k+1} \Phi^{k+1} - \Phi^{k+1} \Theta^{k+1} (\Phi^{k+1}) \right]. \end{aligned} \quad (11)$$

The operator  $I_{k+1}^k$  is the restriction operator from  $k+1$  level to  $k$  level. The defect correction is zero in the fine grid level. If the exact solution from the fine grid level is inserted into the coarse grid  $\tau^k$  equation, it is easy to see that an identity is obtained. This formulation thus satisfies the important condition of zero correction at convergence.

$\Phi$  in  $k+1$  level is corrected from  $k$  level by the following equation:

$$\Phi^{k+1} = \Phi^{k+1} + I_k^{k+1} \left( \Phi^k - I_{k+1}^k \Phi^{k+1} \right), \quad (12)$$

where  $I_k^{k+1}$  is the interpolation operator from  $k$  level to  $k+1$  level. A linear interpolation is used in our work.

We modify Eq. (9) in an overrelaxation form with a shift parameter  $\mu$  [34] as follows:

$$\Phi^{new} = \Phi^{old} + \omega \left( \tau + \Phi^{old} \Theta^{old} - H \Phi^{old} \right) / (D - \mu), \quad (13)$$

where  $D$  is the diagonal term in the discretized Hamiltonian,  $\omega$  is the overrelaxation parameter, it satisfies  $0 < \omega < 2$ . In our calculations, we use  $\mu = 0$  and  $\omega = 1.7$  in the fine grid level,  $\mu = -20$  and  $\omega = 1.0$  in the coarse grid level.

In this local optimized-orbital basis, the orthogonalization step is removed, but the relaxation step in Eq. (13) is more complicated and expensive. This relaxation scales as  $N(R/h)^3$ , where  $R$  is the localization radius and  $h$  the grid spacing. The computational time is reduced as  $R$  decreases. But this speedup is at the cost of accuracy, The convergence rate is stalled when small  $R$  is used [43].

*Green's function*

Let us consider our extended molecule composed of a molecule  $M$  connected to two semi-infinite gold leads, left  $L$  and right  $R$ , respectively. The transmission function is given as [25, 63, 64]

$$T(E) = Tr(\Gamma_L G_M \Gamma_R G_M^\dagger), \quad (14)$$

where  $G_M$  is Green's function of the molecule,  $\Gamma_{L,R}$  are coupling functions between the molecule and the left( $L$ ) and ( $R$ ) leads.  $G_M$  can be expressed as

$$G_M = [E S_M - H_M - \Sigma_L - \Sigma_R]^{-1}, \quad (15)$$

where  $E$  is the electron energy,  $H_M$  and  $S_M$  are the Hamiltonian and overlap matrices for the local optimized-orbitals in the molecule, respectively.  $\Sigma_{L,R}$  are the self-energy terms which are the interactions between the extended molecule and the semi-infinite leads. The self energies are

$$\Sigma_L = (E S_{LM} - H_{LM})^\dagger g_L (E S_{LM} - H_{LM}), \quad (16)$$

$$\Sigma_R = (E S_{RM} - H_{RM})^\dagger g_R (E S_{RM} - H_{RM}), \quad (17)$$

where  $H_{LM}(H_{RM})$  and  $S_{LM}(S_{RM})$  are the Hamiltonian and overlap matrices between the molecule and the left(right) leads for the local optimized-orbitals in the extended molecule, respectively.  $g_L(g_R)$  is the surface Green's function for the left(right) semi-infinite lead. The coupling functions are given as

$$\Gamma_{L,R} = i[\Sigma_{L,R} - \Sigma_{L,R}^\dagger]. \quad (18)$$

The surface Green function can be expressed in terms of principal layers with nearest-neighbor interactions [68, 69]. For a gold lead, it is known that the local density of states is s-band dominated and almost constant near the Fermi level [11, 68]. So  $g_L(g_R)$  can be approximately written as a diagonal matrix with each element proportional to the local density of states [11, 30]. Our calculation is based on the local density states as a function of energy from the reference [68].

## Numerical Results

We use the Landauer formula to calculate the applied bias once the transmission coefficients are known for a range of energies,

$$I(V) = 2 \int_{-\infty}^{\infty} dE T(E, I) \left( \frac{1}{\exp[(E - \mu_L)/kT] + 1} - \frac{1}{\exp[(E - \mu_R)/kT] + 1} \right), \quad (19)$$

where  $\mu_L$  and  $\mu_R$  are the chemical potentials in the left and right lead, respectively. They are defined to be,  $\mu_L = \epsilon_F + V/2$  and  $\mu_R = \epsilon_F - V/2$ , where  $\epsilon_F = -5.31$  eV is the Fermi energy of the gold metal (negative of the bulk gold work function). The applied bias is satisfied by  $\mu_L - \mu_R = V$ .

The geometry optimization of the benzene-1,4-dithiolate molecule (HS-C<sub>6</sub>H<sub>4</sub>-SH) (BDT) is implemented by Gaussian 98 program at SVWN/6-31g(d) level [32]. It is assumed that a dithiol molecule, such as BDT, sandwiched between two Au(111) surfaces loses the hydrogens at both thiol terminations and the sulfur atom of the resulting radical binds strongly to the gold surface [26]. The sulfur atom sits in the center of the triangular pad of the three gold atoms, the distance between sulfur and gold surface is 1.9 Å. The extended BDT molecule is Au<sub>3</sub>-S-C<sub>6</sub>H<sub>4</sub>-S-Au<sub>3</sub>.

Our calculations have been carried out using the real space pseudopotential [66, 67]. Pseudopotentials are used for Au, S, C, and H atoms. Valence states include 6 *s* for Au, 2 *s* and 2 *p* for C, 3 *s* and 3 *p* for S. There are 28 local optimized-orbitals in our calculations. The matrix sizes of  $G_M$  and  $g_L$  are 22 and 3, respectively.

To evaluate the accuracy of the localization approximation, we first tested our solver with and without localization constraints for the Au-BDT-Au molecule. 12th order finite difference representation was used and three grid levels were utilized comprising  $29 \times 15^2$ ,  $57 \times 29^2$  and  $113 \times 57^2$  total points. Figure 1 shows the convergence rates for different methods in the Au-BDT-Au molecule. The fastest convergence is the Ritz method with orthogonalization, which has no localization constraint. The convergence rates from localization constraints depend on the localization radii  $R$ . The larger  $R$ , the faster the convergence rate is. The localization constraints confine the orbitals in their localized regions, so the computed corrections have to be truncated in the iteration process. The more truncated part, the more iterations need to reach a given precision. 40 iterations are needed to reach a precision of  $3 \times 10^{-3}$  for  $R = 11$ . A precision of  $3 \times 10^{-3}$  is sufficient for the quantum transport calculations [43].  $R = 11$  also makes no overlap between the left Au electrode and the right Au electrode. So we will use  $R = 11$  for our transport calculations.

The calculation process is as follows: For a given current, solve Kohn-Sham equations with a current constraint under the optimized-orbital basis with  $R = 11$ . When they converge,  $T(E, I)$  is constructed from Eq. (14). Then the corresponding bias is calculated from Eq. (19). Repeat the above process for next current point.

Figure 2 shows transmission coefficients at currents of 0.0, 13.2, 53.0, and 79.5  $\mu$ A, which correspond to the voltages of 0.0, 1.1, 2.5, 3.8 V, respectively. The main features of the transmission coefficient are 4 discrete sharp peaks close to the Fermi level within  $\pm 2$  eV energy range. 3 peaks are due to the occupied molecular levels, one peak is due to the unoccupied one. As bias increases, the peak positions shift closer to the Fermi level and the peak magnitude change also. When current changes, it causes the charges redistribute, thus modify the potential and the energy levels. The energies of LUMO, HOMO, HOMO-1, HOMO-2 are well separated and slightly shifted in energy by interacting with the gold surface. They match the positions of the peaks in figure 2.

Figures 4 and 5 show the current-voltage characteristics and corresponding differential

conductance in the bias range from -4.3 to 4.3 V. Because the device structure is symmetric, the current-voltage and the differential conductance-voltage are also symmetric. In the small bias range, the current-voltage curve is close to linear. As bias increases, the conductance increases as the HOMO related transmission peak gradually falls into the bias window. This leads to the first conductance peak at  $V = 1.2$  V. As the bias increases further, the HOMO related transmission decreases, so does the conductance. At higher bias, the LUMO and HOMO-1 related transmission peaks fall into the bias window almost at the same time to lead to the second conductance peak at  $V = 2.4$  V. The second conductance peak is stronger than the first one, because they are contributed by two sharper transmission peaks.

It is reasonable to compare our results with other first principles calculating results [20, 26, 29]. The main difference is that different approximations for the Au electrodes. Di Ventura et al [20] applied the jellium model for the Au electrodes. Xue et al [26] used 6 Au atoms as an electrode, Stokbro et al [29] used a self-assembled monolayers with  $(3 \times 3)$  periodicity as an electrode. In the latter two cases the BDT molecule was absorbed in a 3-fold hollow site. Our structure is similar to Xue's structure except 3 Au atoms as an electrode. Our current-voltage curve and conductance-voltage curve are in the same magnitudes as these 3 approaches, the main features are similar, but the qualitative details are different. Our zero bias transmission coefficient is in rough agreement with that of Xue et al, most of our peaks are narrower and positions are slightly shifted. The difference may be due to the following reasons. Xue et al used DFT-SLDA within the generalized-gradient approximation, while we use DFT-LDA. We also use different pseudopotential for Au atom. These differences can shift molecular energy levels. They used the surface Green function in terms of principal layers with nearest-neighbor interactions, while we neglect its off-diagonal term contribution. We may underestimate the coupling interaction with the gold surface, this can result in narrower peaks in the transmission coefficient.

There is a big discrepancy between our calculation and experiment. Our calculation produces two orders of magnitude larger than experiment [1] in current and conductance. Other theoretical calculations showed similar results [20, 26, 29]. The possible reasons to cause the discrepancy between theory and experiment were discussed by those authors [20, 26, 29]. One reason is that a different contact geometry in the experiment than the hollow site used in our calculation. Another reason is the questionable application of DFT-LDA in the electron transport. Solomon et al [70] showed that current and conductance would be in the same magnitudes of the experiment if the spin-restricted open-shell DFT formalism was used instead of the close-shell counterpart. There are additional effects in the experiment such as temperature effect, disorder effect in the Au electrodes near the contacts, which have not been considered in our calculation.

## Summary

In this paper we have described a method to calculate the current-voltage characteristics of a molecule electronic device. A current constrained term is introduced as an imaginary

potential in the conventional DFT. This allows us to handle the open system in nonequilibrium steady state as a closed system. Multigrid technique is used to accelerate convergence in a local optimized-orbital basis. Transmission coefficients are obtained from the Green's function method. Landauer formula is used to calculate the potential bias. The current-voltage characteristics of a BDT extended molecule is studied and our results are comparable to other theoretical calculations. This efficient method provides another way to study the quantum transport of molecule electronic devices.

## Acknowledgments

We gratefully acknowledge the support of the National Science Foundation (CHE-0112322) for this research. We also thank Dr. Kosov and Dr. Fattebert for many helpful discussions.

## References

- [1] M. A. Reed, C. Zhou, C. J. Muller, T. P. Burgin, and J. M. Tour, *Science* **278**, 252 (1997).
- [2] J. Chen, M. A. Reed, A. M. Rawlett, and J. M. Tour, *Science* **286**, 1550 (1999).
- [3] J. C. Ellenbogen and J. C. Love, *Proc. of the IEEE* **88**, 386 (2000).
- [4] M. A. Reed, J. Chen, A. M. Rawlett, D. W. Price, and J. M. Tour, *Appl. Phys. Lett.* **78**, 3735 (2001).
- [5] R. Landauer, *Phil. Mag.* **21**, 863 (1970).
- [6] M. Büttiker, Y. Imry, R. Landauer, and S. Pinhas, *Phys. Rev. B* **31**, 6207 (1985).
- [7] Y. Imry and R. Landauer, *Rev. Mod. Phys.* **71**, 306 (1999).
- [8] V. Mujica, M. Kemp, and M. A. Ratner, *J. Chem. Phys.* **101**, 6849 (1994).
- [9] V. Mujica, M. Kemp, and M. A. Ratner, *J. Chem. Phys.* **101**, 6856 (1994).
- [10] S. Datta, W. Tian, S. Hong, R. Reifenberger, J. I. Henderson, and C. P. Kubiak, *Phys. Rev. Lett.* **79**, 2530 (1997).
- [11] W. Tian, S. Datta, S. Hong, R. Reifenberger, J. I. Henderson, and C. P. Kubiak, *J. Chem. Phys.* **109**, 2874 (1998).
- [12] E. G. Emberly and G. kirczenow, *Phys. Rev. B* **58**, 10911 (1998).
- [13] M. A. Ratner, B. Davis, M. Kemp, V. Mujica, A. Roitberg, and S. Yaliraki, in *Molecular Electronics: Science and Technology* (A. Aviram and M. A. Ranter, eds, NY Acad. Sci.), **852**, 22 (1998).
- [14] S. N. Yaliraki and M. A. Ratner, *J. Chem. Phys.* **109**, 5036 (1998).
- [15] S. N. Yaliraki, M. Kemp, and M. A. Ratner, *J. Am. Chem. Soc.* **121**, 3428 (1999).
- [16] S. N. Yaliraki, A. E. Roitberg, C. Gonzalez, V. Mujica, and M. A. Ratner, *J. Chem. Phys.* **111**, 6997 (1999).
- [17] V. Mujica, A. E. Roitberg, and M. A. Ratner, *J. Chem. Phys.* **112**, 6834 (2000).
- [18] L. E. Hall, J. R. Reimers, N. S. Hush, and K. Silverbrook, *J. Chem. Phys.* **112**, 1510 (2000).
- [19] N. D. Lang, *Phys. Rev. B* **52**, 5335 (1995).
- [20] M. Di Ventra, S. T. Pantelides, and N. D. Lang, *Phys. Rev. Lett.* **84**, 979 (2000).

- [21] M. Di Ventura and N. D. Lang, Phys. Rev. B. **65**, 45402 (2001).
- [22] R. G. Parr and W. Yang, *Density-Functional Theory of Atoms and Molecules*, (Oxford University Press, Oxford, 1989).
- [23] J. Taylor, H. Guo, and J. Wang, Phys. Rev. B **63**, 245407 (2001).
- [24] Y. Xue, S. Datta, and M. A. Ratner, J Chem. Phys. **115**, 4292 (2001).
- [25] Y. Xue, S. Datta, and M. A. Ratner, Chem. Phys. **281**, 151 (2002).
- [26] Y. Xue and M. A. Ratner, Phys. Rev. B **68**, 115406 (2003).
- [27] P. S. Damle, A. W. Ghosh, and S. Datta, Chem. Phys. **281**, 171 (2002).
- [28] M. Brandbyge, J.-L. Mozos, P. Ordejón, J. Taylor, and K. Stokbro, Phys. Rev. B **65**, 165401 (2002).
- [29] K. Stokbro, J. Taylor, M. Brandbyge, J.-L. Mozos, and P. Ordejón, Comp. Mat. Sci. **27**, 151 (2003).
- [30] P. A. Derosa and J. M. Seminario, J. Phys. Chem. **105**, 471 (2001).
- [31] J. Tomfohr and O. F. Sankey, J. Phys. Chem. **120**, 1542 (2004).
- [32] M. J. Frisch, G. W. Trucks, H. B. Schlegel *et al.* GAUSSIAN 98, Revision A. 7 (Gaussian, Inc., Pittsburgh, PA, 1998).
- [33] N. Wijesekera, G. Feng, and T. L. Beck, J. of Theor. Comput. Chem. **2**, 1 (2003).
- [34] N. Wijesekera, G. Feng, and T. L. Beck, in preparation
- [35] D. S. Kosov and J. C. Greer, Phys. Lett. A **291**, 46 (2001).
- [36] D. S. Kosov, J. Chem. Phys. **116**, 6368 (2002).
- [37] D. S. Kosov, [xxx.lanl.gov/abs/con-mat/0308105](http://xxx.lanl.gov/abs/con-mat/0308105)
- [38] D. P. Sánchez-Portal, P. Ordejón, E. Artacho, and J. M. Soler, Intl. J. Quantum Chem. **65**, 453 (1997).
- [39] M. Challacombe, Comput. Phys. Commun. **128**, 93 (2000).
- [40] M. Payne, M. Teter, D. Allan, T. Arias, and J. Joannopoulos, Rev. Mod. Phys. **64**, 1045 (1992).
- [41] T. L. Beck, Rev. Mod. Phys. **72**, 1041 (2000).
- [42] S. Goedecker, Rev. Mod. Phys. **71**, 1085 (1999).

- [43] J.-L. Fattebert and J. Bernholc, Phys. Rev. B **62**, 1713 (2000).
- [44] J.-L. Fattebert, J. Comput. Phys. **149**, 75 (1999).
- [45] T. L. Beck, J. Comput. Chem. **20**, 1731 (1999).
- [46] E. L. Briggs, D. J. Sullivan, and J. Bernholc, Phys. Rev. B **54**, 14362 (1996).
- [47] T. Hoshi and T. Fujiwara, J. Phys. Soc. Jpn. **66**, 3710 (1997).
- [48] N. A. Modine, G. Zumbach, and E. Kaxiras, Phys. Rev. B **55**, 10289 (1997).
- [49] F. Ancilotto, P. Blandin, and F. Toigo, Phys. Rev. B **59**, 7868 (1999).
- [50] I.-H. Lee, Y.-H. Kim, and R. M. Martin, Phys. Rev. B **61**, 4397 (2000).
- [51] J. Wang and T. L. Beck, J. Chem. Phys. **112**, 9223 (2000).
- [52] M. Heiskanen, T. Torsti, M. J. Puska, and R. M. Nieminen, Phys. Rev. B **63**, 245106 (2001).
- [53] G. Wachutka, Phys. Rev. B **34**, 8512 (1986).
- [54] K. Hirose, M. Tsukada, Phys. Rev. B **51**, 5278 (1995).
- [55] H. J. Choi and J. Ihm, Phys. Rev. B **59**, 2267 (1999).
- [56] D. Embriaco and G. C. La Rocca, Solid State Communications **117**, 407 (2001).
- [57] W. Frensley, Rev. Mod. Phys. **62**, 745 (1990).
- [58] C. Lent and D. Kirkner, J. Appl. Phys. **67**, 6353 (1990).
- [59] D. Mamaluy, M. Sabathil, and P. Vogl, J. App. Phys. **93**, 4628 (2003)
- [60] Y. Fujimoto and K. Hirose, Nanotechnology **14**, 147 (2003).
- [61] Y. Fujimoto and K. Hirose, Phys. Rev. B **67**, 195315 (2003).
- [62] S. Okano, K. Shiraishi, and A. Oshiyama, Phys. Rev. B **69**, 045401 (2004).
- [63] S.datta, *Electroic Transport in Mesoscopic Systems* (Cambridge University Press, Cambridge, 1995).
- [64] M. B. Nardelli, J.-L. Fattebert, and J. Bernholc, Phys. Rev. B **64**, 245423 (2001).
- [65] S. H. Vosko, L. Wilk, and M. Nusair, Can.J. Phys. **58**, 1200 (1980).
- [66] S. Goedecker, M. Teter, and J. Hutter, Phys. Rev. B **54**, 1703 (1996).

- [67] C. Hartwigsen, S. Goedecker, and J. Hutter, Phys. Rev. B **58**, 3641 (1998).
- [68] Y. Xue, Ph. D. thesis, Purdue University, (2000).
- [69] M. B. Nardelli, Phys. Rev. B **60**, 7828 (1999).
- [70] G. C. Solomon, J. R. Reimers, and N. S. Hush , J. Chem. Phys. **121**, 6615 (2004).

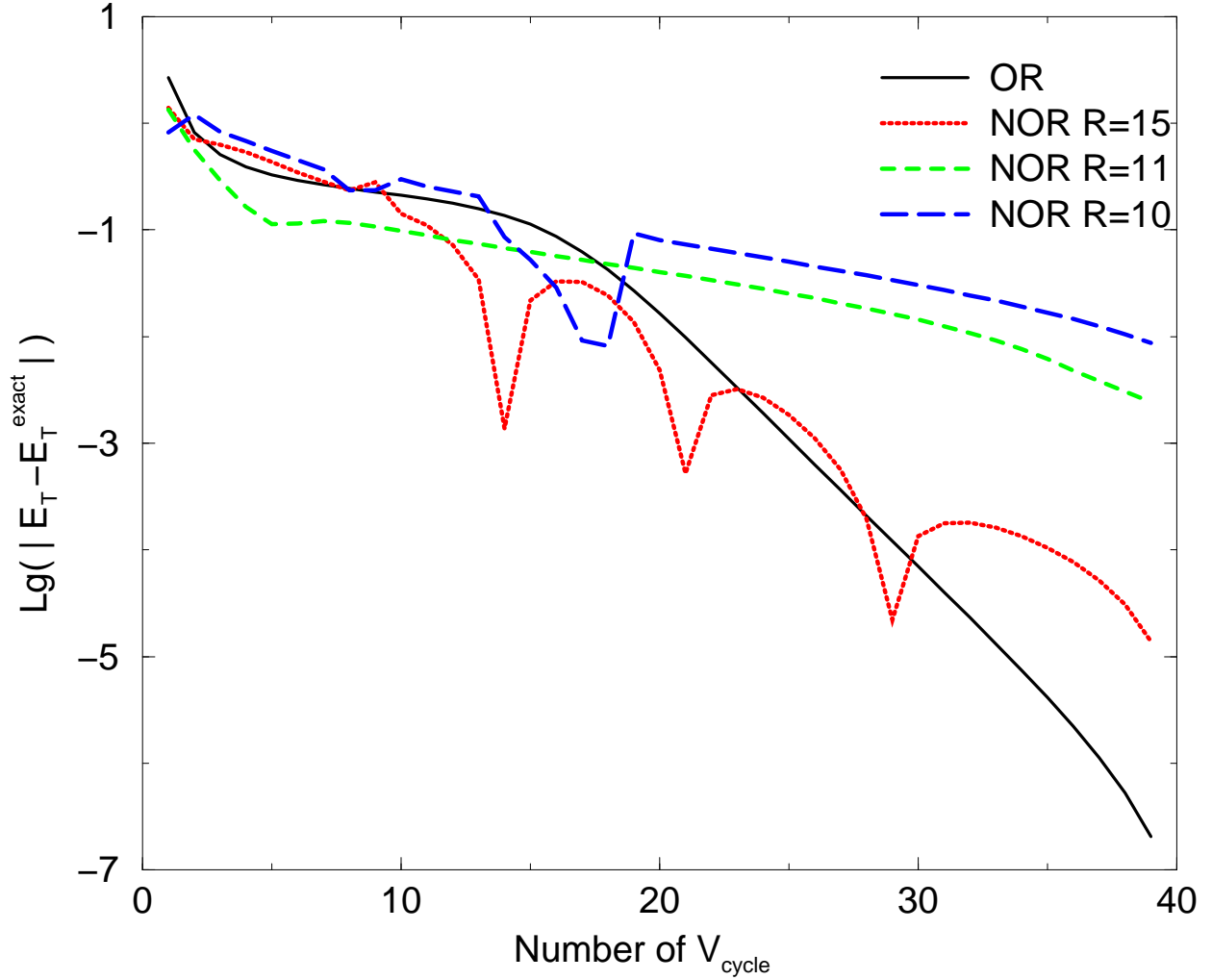


Figure 1: Convergence rates for different methods in the Au-BDT-Au device. The logarithm (base 10) of the difference between the current and fully converged total energies is plotted against the number of V-cycles (self-consistency iterations). The solid line is the result of the Ritz method with orthogonalization, others are the results from nonorthogonal optimized-orbital multigrid method with different localization radii in atomic unit. The fine grid spacing is  $h = 0.25$ .

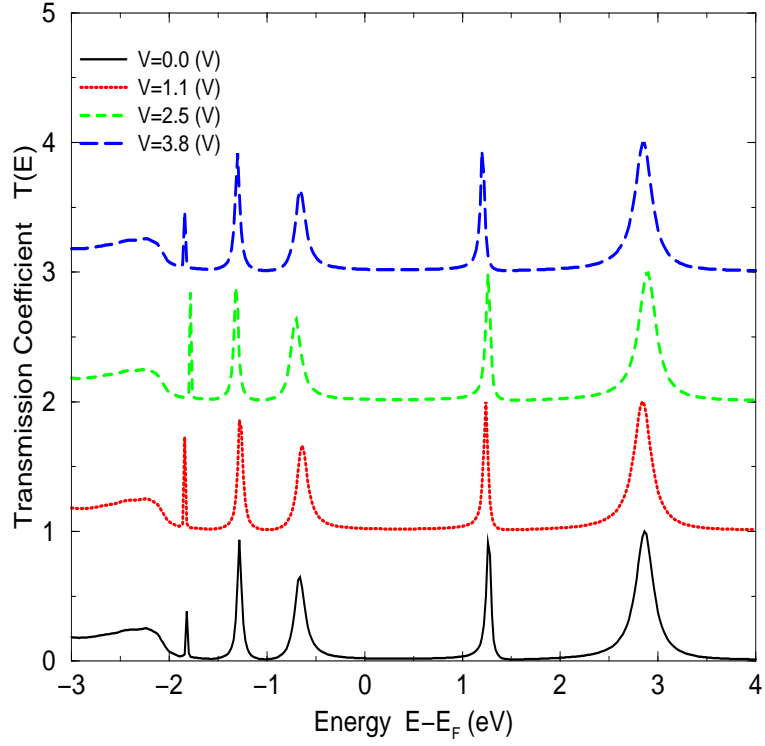


Figure 2: Current-induced variation of transmission coefficient for the Au-BDT-Au device at currents of 0.0, 13.2, 53.0, and 79.5  $\mu\text{A}$ , which correspond to the voltages of 0.0, 1.1, 2.5, and 3.8 V, respectively. Each upper curve is shifted by 1 from the bottom one.

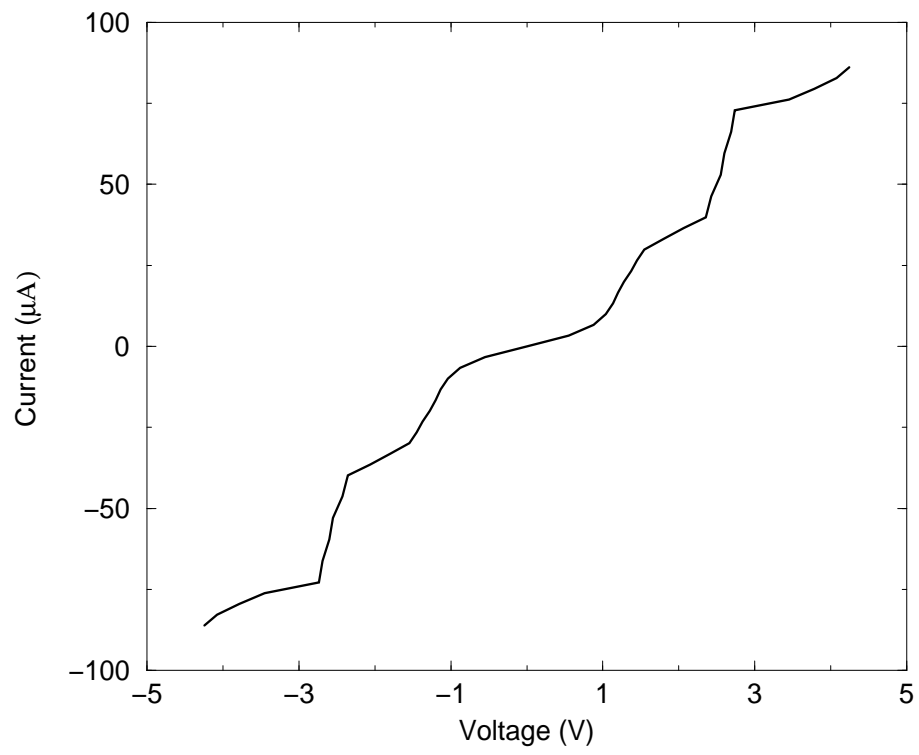


Figure 3: I-V characteristics of the Au-BDT-Au device

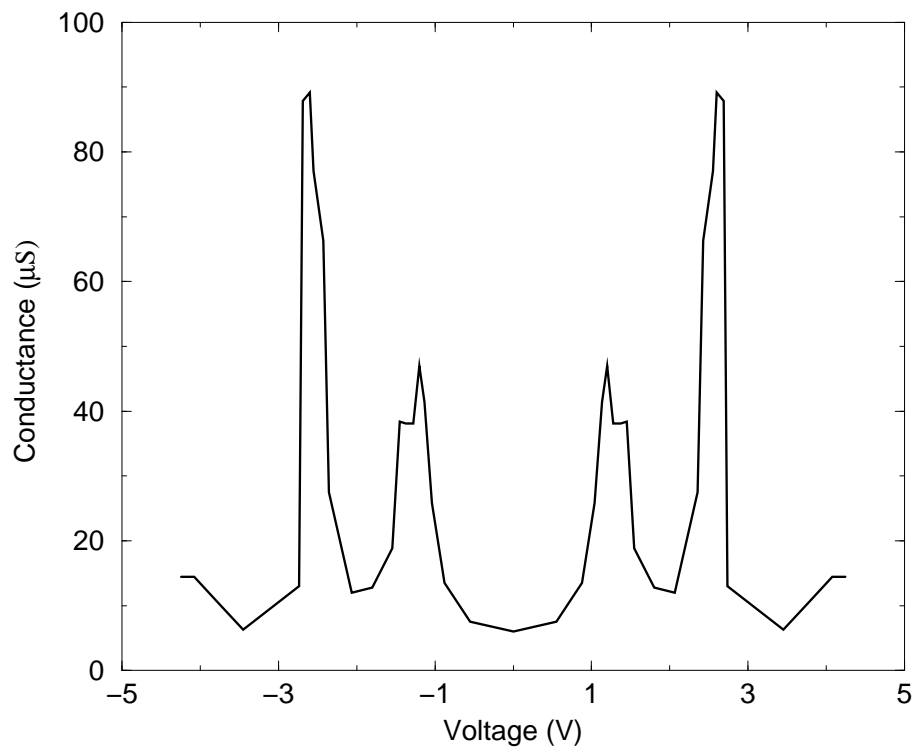


Figure 4: Differential conductance characteristics of the Au-BDT-Au device